Fifth International Conference on CFD in the Process Industries
CSIRO, Melbourne, Australia
13-15 December 2006

CFD ANALYSIS OF IMPINGING AXISYMMETRIC TURBULENT FOUNTAINS

Ajit GODBOLE[1] , Paul COOPER[1], John NORRISH[1] and Gary R. HUNT[2]

[1]School of Mechanical, Materials and Mechatronic Engineering, University of Wollongong, NSW 2522, Australia.
[2]Department of Civil and Environmental Engineering, Imperial College London, London, SW7 2AZ, UK.

ABSTRACT

When a positively buoyant vertical fluid jet directed downwards from its source impinges on a horizontal flat surface, the resulting flow is termed an "impinging fountain". These flows arise in a number of practical situations, for example, in gas metal arc welding (GMAW). Developing a description of this flow presents the researcher with a number of challenges and forms the motivation for this work.

In this paper, CFD simulations of impinging fountain flows in a brine environment are presented, and the predictions compared with earlier experimental work carried out by two of the authors (Cooper and Hunt, 2004). Close agreement is achieved between experiment and simulation. In particular, the CFD accurately predicts the lateral spread of the impinging fountain along the horizontal surface. This spread determines the initial size of the source of the buoyant plume that is subsequently formed and is, thus, a crucial parameter in predicting the spread of pollutants, such as welding fume, via the plume.

The results presented herein are a precursor to theoretical and experimental investigations of GMAW-induced flow fields by the authors.

NOMENCLATURE

B	Buoyancy Flux	(m^4/s^3)
D	Diameter	(m)
Fr	Froude Number	
g	Gravitational Acceleration	(m/s^2)
H	Standoff Distance	(m)
L	Length Scale	(m)
M	Momentum Flux	(m^4/s^2)
m	Mass Fraction of Salt	
p	Pressure	(Pa)
Q	Volume Flow Rate	(m^3/s)
R	Radial Distance	(m)
$\boldsymbol{u}$	Velocity Vector	(m/s)
V	Average Velocity	(m/s)
v,w	Velocity Components along y, z axes	(m/s)
ρ	Density	(kg/m^3)
ϕ	General Conserved Variable	
μ	Dynamic Viscosity	(Pa-s)

INTRODUCTION

Buoyancy-driven convective flows abound in the natural and artificial environments. An understanding of the structure of these flows is of interest from both theoretical and practical points of view. In plumes, buoyancy and momentum fluxes at the source act in the same direction, as in the case of thermal plumes arising from an upward injection of warm air in a cooler environment. Flows that develop from sources of buoyancy and momentum fluxes that act in opposite directions are known as "fountains" (e.g. Turner, 1966). These flows result from a combination of forced and natural convective effects, and are encountered in a number of industrial and natural settings. In industrial workplaces, for example, warm (positively buoyant) air curtains formed by jets directed downward from the ceiling give rise to turbulent fountains. Flows induced by the gas metal arc welding (GMAW) process bear a close resemblance to impinging fountain flows, as established by Norrish, et al. (2005). On a different scale and in a different setting, the jets formed by V-STOL aircraft engines are an example of similar flows. Common to these examples is a positively buoyant jet directed downward from a source in the vicinity of a horizontal surface (the ground in the case of air curtains and V-STOL aircraft; the surface of the workpiece in the case of GMAW-induced flows). In the absence of density differences, the impinging *jet* flow (as opposed to *fountain*) is relevant to the cooling of microelectronic components (e.g. Chiriac and Ortega, 2002).

The descending jet-like flow from the fountain source initially impinges on the horizontal surface and is forced to travel radially outward. After having travelled a certain distance along the surface, the buoyancy force becomes dominant, causing the flow to detach from the surface and rise up, forming the source of a thermal plume. Of concern in the case of GMAW-induced flows are the welding fume and other gaseous/particulate contaminants transported by the plume into the breathing zone of operators. If the spread of contaminants via impinging fountain flows is to be controlled effectively, it is necessary to understand and predict the structure of these flows.

FLOW STRUCTURE

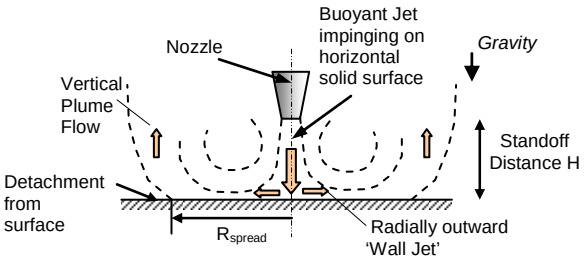

Figure 1: Schematic diagram of impinging fountain.

In an impinging fountain flow, a vertical positively buoyant stream impinges on a horizontal surface, and is re-directed along the surface (Figure 1). The resulting horizontal flow is termed the 'wall jet' (e.g. Rajaratnam, 1976). Frictional shear along the surface slows down the flow in the horizontal direction. Additionally, the flow is subjected to a buoyancy force. Hence, as the flow proceeds outward along the surface, the buoyancy force becomes progressively more dominant. As a result the flow separates from the plate at a particular radial distance resulting in a rising thermal plume.

Determining the outward (radial) spread of the wall jet (R_{spread} in Figure 1) is relevant from the point of view of controlling the spread of contaminants that may be carried by the plume. This radial spread will influence the initial source size of the ascending plume flow and, hence, the propensity of the plume to convey contaminants with it. The magnitude of R_{spread} is dependent upon a three-way competition between the forces of inertia (originally imparted by the nozzle), friction (due to the adjacent impermeable horizontal surface), and buoyancy (due to the density difference between the wall jet fluid and the ambient). Two of the present authors (Cooper and Hunt, 2004) have previously conducted experimental investigations of impinging axisymmentric fresh water fountains created in a large glass tank filled with brine. They showed that, suitably scaled, their experimental measurements of R_{spread}, collapsed onto a single curve (R_{spread}/H, plotted as a function of the source Richardson Number).

Fountain Source Conditions

The nozzle (fountain source) flow is defined in terms of the volume flux Q_{source}, buoyancy flux B_{source} and specific momentum flux M_{source} (e.g. Turner, 1966). From dimensional considerations, these parameters can be combined to define a 'jet length' L_{jet} and an 'acceleration length' L_{accl} :

$$L_{jet} = \frac{M_{source}^{3/4}}{B_{source}^{1/2}} \quad (1)$$

$$L_{accl} = \frac{Q_{source}}{M_{source}^{1/2}} \quad (2)$$

The source Froude number and the source Richardson number are then

$$Fr_{source} = \frac{L_{jet}}{L_{accl}} \quad (3)$$

$$Ri_{source} = \left(\frac{1}{Fr_{source}}\right)^2 \quad (4)$$

EXPERIMENTAL ARRANGEMENT

The experiments were conducted in a large square base glass visualisation tank filled with saline solution. Into this, a downward-directed fresh water jet was introduced at different distances (25 mm to 200 mm) from a solid horizontal surface, using nozzles of different diameters (3 mm to 10 mm). The nozzles were located at the bottom of a slender cylindrical support fixed precisely in the middle of the tank. Initially, the flow field was visualised using a shadowgraph. Further experiments were conducted with the source fluid laced with sodium fluorescein and with the tank lit from below with a light sheet passing through the axis of symmetry. This Light-Induced Fluorescence (LIF) technique allowed the internal flow structure of an impinging fountain to be clearly visualised. The light sheet was generated by means of a line of dichroic incandescent 12v bulbs that were directed at a 1mm wide slit in black cardboard sheeting attached to the lower glass surface of the tank. It is estimated that the light sheet varied in thickness between 2 and 3mm over the field of view. Images were captured by means of a digital CCD video camera (JAI CV-M4 monochrome, 1380(h) × 1030(v) pixel read out) and processed using the DigiFlow software system (Dalziel, 1993).

CFD SIMULATIONS

Computational Domain and Mesh

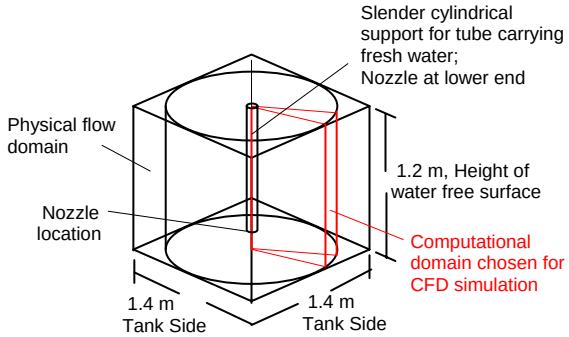

Figure 2: Physical and computational domains.

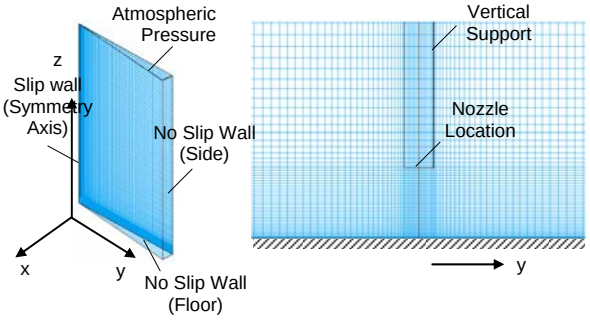

Figure 3: Computational mesh with refinement near floor.

The physical flow domain is shown schematically in Figure 2 together with the corresponding computational domain. The relatively large dimensions of the tank and the small diameters of the nozzles and the cylindrical support made it possible to choose an axisymmetric computational domain. The radial extent of the computational domain was equal to half the tank side, the vertical extent was equal to the height of the free water surface above the tank floor, and the circumferential extent was 0.1 radian. The mesh size was (1, 104, 136) in the x, y and z (θ, r, z) directions, respectively The computational cells are distributed non-uniformly with denser cell populations in regions where large gradients in flow parameters are expected.

Governing Differential Equations

The flow was modelled as single phase, with the fluid density a function of the local salt concentration. Equations of conservation of mass and momentum were solved iteratively until convergence was achieved.

The general conservation equation can be expressed in terms of the general variable ϕ as (e.g. Patankar, 1980):

$$\frac{\partial}{\partial t}(\rho\phi) + div(\rho \boldsymbol{u}\phi - \Gamma_\phi grad\phi) = S_\phi \qquad (8)$$

The variable ϕ, the diffusion coefficient Γ_ϕ, and the source term S_ϕ assume different values depending upon the meaning of the conserved variable:

Conservation of Mass(saline water)

Here, $\phi = 1$; $\Gamma_\phi = 0$ and $S_\phi = 0$, giving

$$\frac{\partial}{\partial t}(\rho) + div(\rho \boldsymbol{u}) = 0 \qquad (9)$$

Conservation of Mass(salt)

Here, $\phi = m$; $\Gamma_\phi = 0$ and $S_\phi = 0$, giving

$$\frac{\partial}{\partial t}(\rho m) + div(\rho \boldsymbol{u} m) = 0 \qquad (10)$$

Momentum Equations (y and z directions)

Here, $\phi = v, w$; $\Gamma_\phi = \mu$, and

$S_\phi = -\frac{\partial p}{\partial y, z} + BF_{y,z} + VF_{y,z}$, so that

$$\frac{\partial}{\partial t}\left(\rho \frac{v}{w}\right) + div\left(\rho \boldsymbol{u} \frac{v}{w} - \mu\, grad \frac{v}{w}\right) = S_\phi \qquad (11)$$

As the experimental salt concentrations were relatively low, it was assumed that the presence of salt did not affect the viscosity of the fluid significantly. The value of the kinematic viscosity was taken as that of pure water.

In addition, the conservation equation for a tracer (corresponding to the dye in the experiment) introduced at the nozzle inlet and passively conveyed by the source was solved simultaneously, to visualize the spread of the buoyant jet and plume.

Auxiliary Equations

Density variation: The local density of the fluid can be expressed in terms of the local salt concentration as:

$$\rho = \rho_{\substack{fresh \\ water}} + m_{salt}(1000) \qquad (9)$$

where m_{salt} is the mass fraction of salt in the water.

Body force per unit volume

$$BF_y = 0;\ BF_z = -\rho g \qquad (10)$$

where $g = 9.81$ m/s^2.

The standard k-ε turbulence model without gravity correction was used.

Boundary Conditions

The boundary conditions used are shown in Figure 3. The atmospheric pressure boundary condition on the "ceiling" of the computational domain ensures a hydrostatic pressure distribution throughout the body of saline solution. Fresh water ($m_{salt} = 0$) is injected into the saline environment (m_{salt} = experimental value) at a velocity calculated from the experimental conditions for each separate simulation. The symmetry axis (and the vertical sides of the slice) are boundaries "with slip", while the floor and side wall are "no-slip" walls.

Solution Procedure

The governing equations were solved using the control volume technique using a commercially available CFD package (PHOENICS v3.5, 3.6). Both steady state and transient simulations were carried out, and the results were compared with the available experimental data.

COMPARISON OF RESULTS

Quasi-Steady State

Figure 4 shows a typical result in the form of the simulated velocity field in the vicinity of the solid horizontal surface. Note that the vectors in the jet are not shown for greater clarity. The growth of the radial wall jet is predicted to be approximately linear, as observed in the experiments.

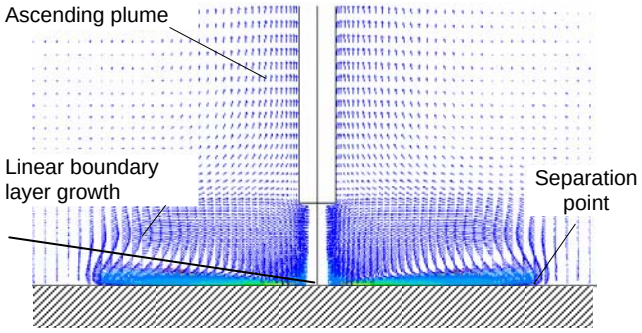

Figure 4: Typical velocity vector field near floor (vectors in the jet region below the nozzle have been omitted for clarity).

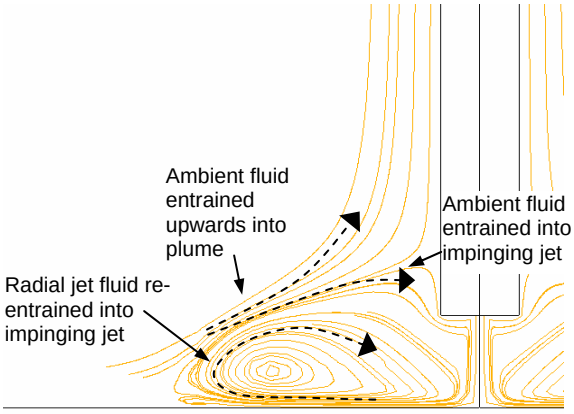

Figure 5: Typical predicted streamline pattern.

Figure 5 shows a typical streamline pattern in the flow field. The formation of a toroidal, vortex-like structure is clearly seen. This leads to some of the buoyant fluid being re-entrained into the radial jet. At the same time, a fraction of the ambient fluid is entrained towards the impinging jet. An upward plume flow is also predicted.

Figures 6a, 7a and 8a show images (snapshots) of the unsteady impinging fountain flow field observed in experiments under three different conditions. These images have been enhanced primarily by correcting the background light intensity using the DigiFlow software (Dalziel, 1993), but not for the progressive attenuation of light intensity from bottom to top, due to the location of the light source below the transparent floor. This makes the flow in the wall jet particularly clear to visualize. However, the grey shades in these images do not represent dye concentration quantitatively.

Figures 6b, 7b and 8b show the results of the CFD simulations in terms of the spread of a passively conveyed tracer (dye), injected with the incoming nozzle flow. The simulation results are shown in the form of time-averaged, normalized dye concentration contours (maximum value 1 at the source).

Table 1 summarizes the conditions under which the experiments were carried out, and also shows a comparison of the observed and predicted values of R_{spread}. It is seen that there is very good agreement between experiment and simulation as far as the radius of spread is concerned for the conditions examined.

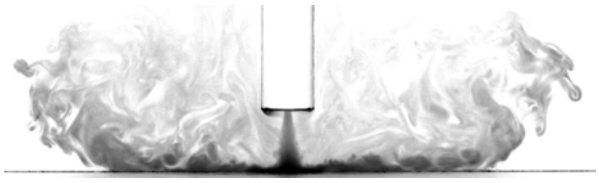

Figure 6a: Impinging fountain spread #1 (experiment). H/L_{jet} = 0.1*;* H/D_{source} = 8.3.

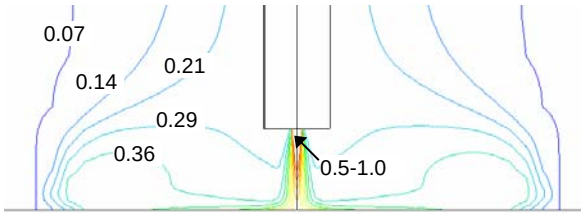

Figure 6b: Impinging fountain spread #1 (Simulation). H/L_{jet} = 0.1*;* H/D_{source} = 8.3.

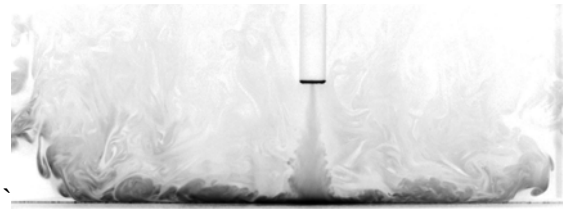

Figure 7a: Impinging fountain spread #2 (experiment). H/L_{jet} = 0.29*;* H/D_{source} = 33.3.

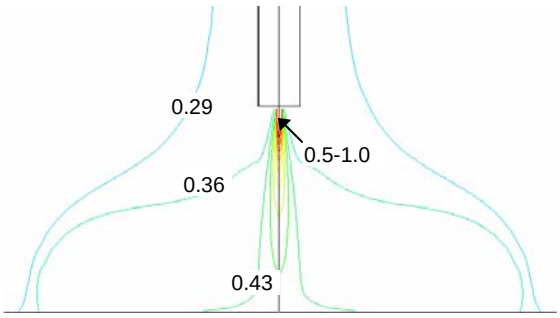

Figure 7b: Impinging fountain spread #2 (simulation). H/L_{jet} = 0.29*;* H/D_{source} = 33.3.

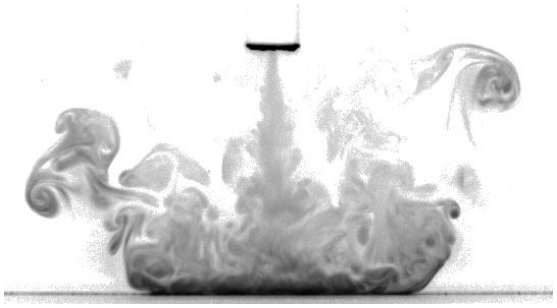

Figure 8a: Impinging fountain spread #3 (experiment). H/L_{jet} = 0.67*;* H/D_{source} = 33.3.

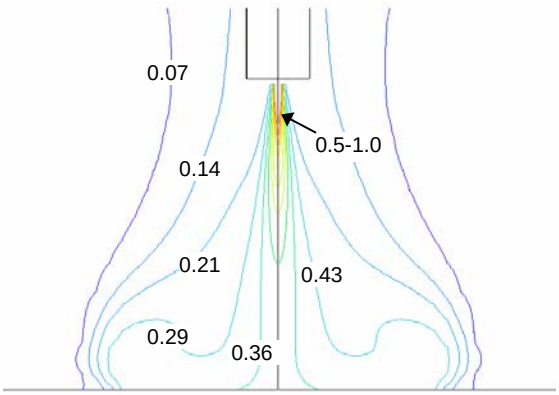

Figure 8b: Impinging fountain spread #3 (simulation). H/L_{jet} = 0.67*;* H/D_{source} = 33.3.

Table 1: Experimental conditions and steady-state results.

	Figures 6a, 6b	Figures 7a, 7b	Figures 8a, 8b
H (mm)	25	100	100
D_{source} (mm)	3	3	3
V_{source}(m/s)	1.33	1.33	0.57
$\rho_{ambient}$ (kg/m^3)	1008.4	1003.3	1003.0
H/L_{jet}	0.1	0.29	0.67
H/D_{source}	8.3	33.3	33.3
$(R_{spread}/D_{source})_{experiment}$	25	45	23
$(R_{spread}/D_{source})_{simulation}$	24	46	23

Transient Behaviour

Cooper and Hunt (2004) used their experimental data to investigate the initial evolution of the impinging fountain flow field before it reached a quasi-steady state. They found that the radius of the base of the plume increased with time in the initial transients after the vertical jet impinged on the horizontal surface, and then decreased to a slightly smaller steady-state value. This observation is of some interest from the point of view of pollutant spread via the starting plume, as it shows that the flow gives rise to an initial 'burst' of contaminant that could be more concentrated than established in the quasi-steady-state case.

A transient CFD simulation was carried out to investigate this behaviour. Figures 9a and 9b show the velocity vector field and the normalized dye concentration field approximately 1 second after the flow is initiated. It is predicted that the ambient fluid in the vicinity of the jet and support is entrained and initially carried downward by the jet. This continues until a time when the toroidal vortex at the interface between the jet fluid and the ambient fluid is close enough to the floor. The initially vertically elongated vortex then spreads out horizontally (see Figure 5), as the jet fluid impinges on the horizontal surface and begins to flow radially outward.

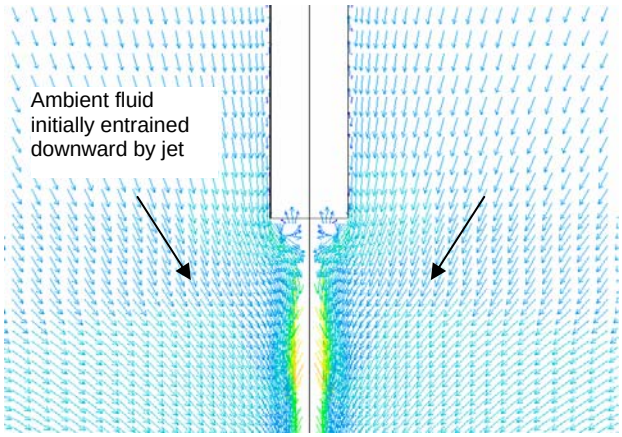

Figure 9a: Velocity vector field ~ 1 s after commencement (simulation). H/L_{jet} = 0.69*;* H/D_{source} = 20.

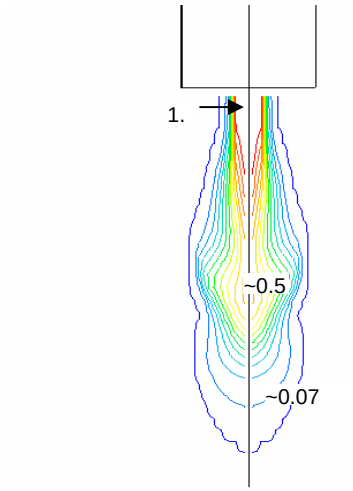

Figure 9b: Dye concentration field ~ 1 s after commencement (simulation). H/L_{jet} = 0.69; H/D_{source} = 20.

Figures 10a and 10b show the velocity vector field in the ambient and the normalized dye concentration field about 5 seconds after commencement of the jet flow.

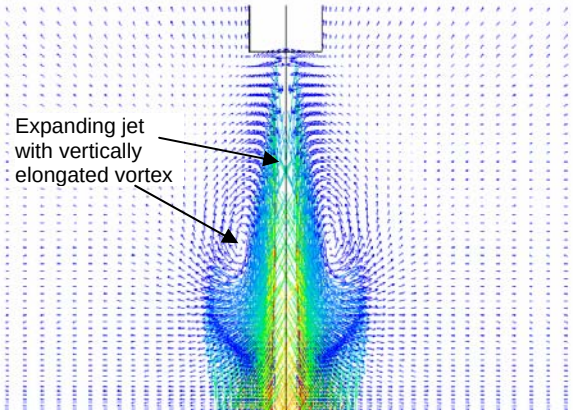

Figure 10a: Velocity vector field ~ 5 s after commencement (simulation). H/L_{jet} = 0.69*;* H/D_{source} = 20.

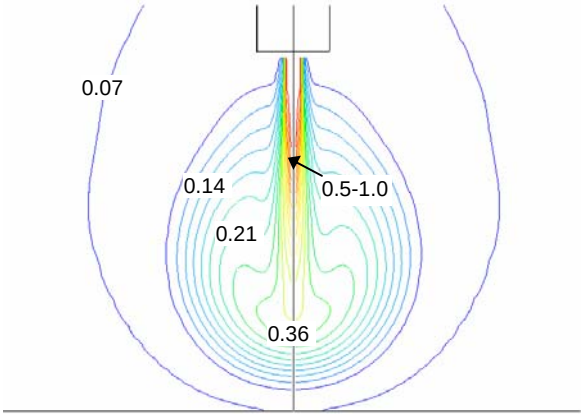

Figure 10b: Dye concentration field ~ 5 s after commencement (simulation). H/L_{jet} = 0.69; H/D_{source} = 20.

After about 10 seconds, the plume becomes strong enough to entrain the ambient fluid consistently in the upward direction. The greater spread of the plume base in the initial transients is well reproduced in the simulation. The point of separation was determined by plotting the variation of the radial velocity component in the cell adjacent to the floor of the computational domain, and noting the radial distance of the point where this component changes sign. This is shown in Figure 11. It is predicted that this point initially moves radially outward, before being drawn back in slightly toward the axis of symmetry, as the plume above the wall jet develops into a steady flow.

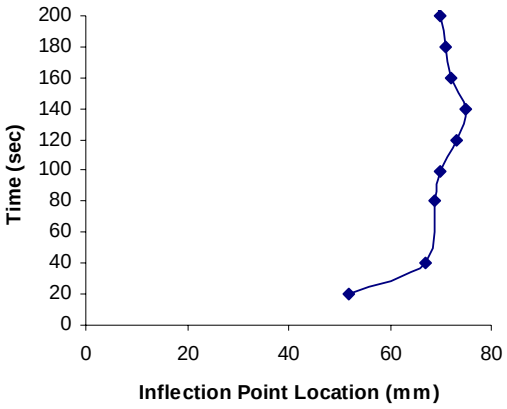

Figure 11: Variation of radius of plume base with time. H/L_{jet} = 0.34; H/D_{source} = 33.3.

Experimentally, R_{spread} determined visually, from the dye concentration field in successive images of the evolving flow. This tends to over-estimate the radius of spread, due to re-entrainment of some of the dye from the ambient into the plume base. An example of the experimentally determined variation of R_{spread} with time is shown in Figure 12.

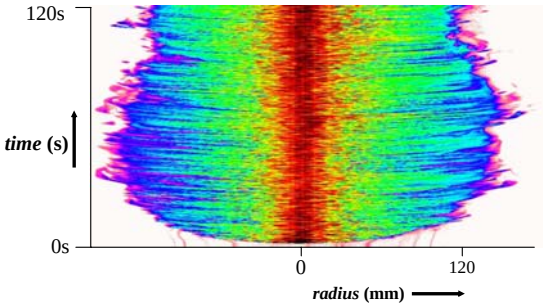

Figure 12: Variation of R_{spread} with time - H/L_{jet} = 0.34; H/D_{source} = 33.3. (Cooper and Hunt, 2006)

CONCLUSION

CFD simulations of impinging fountain flows in a saline water environment were carried out using a commercially available CFD package. This particular study is a precursor to a theoretical and experimental investigation of flows induced by the gas metal arc welding (GMAW) process, although impinging fountain flows occur in many other natural and industrial settings. The results of the simulations were compared with experimental results obtained by two of the present authors. These focussed on the radial spread of the impinging buoyant flow on the horizontal surface under different flow conditions. There was very good agreement between simulations and experiments, especially in the quasi-steady-state simulations. The transient simulations were able to reproduce qualitatively the physical behaviour of the plume that rises from the boundary, whereby the radial spread of the fountain decreases from the initial value to a slightly smaller steady-state value.

REFERENCES

BEJAN, A., (1982), *Entropy generation through heat and fluid flow*, John Wiley and Sons.

CHIRIAC, V.A. and ORTEGA, A., (2002), "A numerical study of the unsteady flow and heat transfer in a transitional confined slot jet impinging on an isothermal surface", *Int. J. Heat and Mass Transfer*, vol. 45, pp 1237-1248.

COOPER, P. and HUNT, G.R., (2004), "Experimental Investigation of Impinging Axisymmetric Turbulent Fountains", *Proc. 15th Australasian Fluid Mechanics Conference*, Sydney, Australia, December.

COOPER, P. and HUNT, G.R., (2006), "Turbulent Impinging Axisymmetric fountains", submitted to *Physics of Fluids, July 2006*.

DALZIEL, S.B., (1993), "Rayleigh-Taylor instability: experiments with image analysis", *Dyn. Atmos. Oceans*, **20**, pp 127-153.

NORRISH, J. COOPER, P., SLATER, G., (2005) "Particulate fume plume distribution and breathing zone exposure in gas metal arc welding", *Proc Int. Conf. on Health and Safety in Welding*, Copenhagen, Denmark.

PATANKAR, S.V., (1980), "Numerical Heat Transfer and Fluid Flow", Hemisphere Publishing, Washington.

RAJARATNAM, N., (1976), "Turbulent Jets", *Elsevier*, New York.

TURNER, J. S., (1966), "Jets and plumes with negative or reversing buoyancy", *J. Fluid Mech.*, **26**, 779-792.